Infinite temperature limit of meson spectral functions calculated on the lattice

F. Karsch, E. Laermann, and S. Stickan
Fakultät für Physik, Universität Bielefeld, D-33615 Bielefeld, Germany

P. Petreczky
Nuclear Theory Group, Physics Department, Brookhaven National Laboratory, Upton, New York 11973, USA
(Received 24 March 2003; published 10 July 2003)

We analyze the cutoff dependence of mesonic spectral functions calculated at finite temperature on Euclidean lattices with a finite temporal extent. In the infinite temperature limit we present analytic results for lattice spectral functions calculated with standard Wilson fermions as well as a truncated perfect action. We explicitly determine the influence of ''Wilson doublers'' on the high momentum structure of the mesonic spectral functions and show that this cutoff effect is strongly suppressed when using an improved fermion action.

DOI: 10.1103/PhysRevD.68.014504 PACS number(s): 12.38.Gc, 11.10.Wx, 12.38.Mh, 25.75.Nq

I. INTRODUCTION

The thermal modification of the basic properties of hadrons, e.g., their masses and decay widths, is one of the central issues in the discussion of experimental signals that can emerge from the dense partonic systems created in heavy ion collisions. Lattice calculations can, in principle, provide this information through the analysis of the thermal properties of Euclidean correlation functions of suitably chosen operators carrying hadronic quantum numbers. These correlation functions contain all the necessary information on the temperature dependence of hadronic spectral functions. In order to make such studies quantitative and to be able to reliably extract information valid in the continuum limit, we have to understand, however, in detail the cutoff dependence of spectral functions calculated on the lattice at finite temperature. We provide here a detailed analysis of mesonic spectral functions in the infinite temperature limit and discuss their cutoff dependence. This provides a basis for discussions of the cutoff dependence of spectral functions at finite temperature and is similar in spirit to studies of the cutoff dependence of the QCD equation of state which were first performed in the ideal gas (infinite temperature) limit [1].

Information on the hadronic spectrum is extracted in lattice calculations from the properties of Euclidean time correlation functions of suitably chosen hadronic currents. A recent suggestion [2] is to apply the maximum entropy method (MEM), a well known statistical tool for the analysis of noisy data [3], to the analysis of these correlation functions also. This opened the possibility of extracting detailed information on hadronic spectral functions $\sigma(\omega,T)$, at zero as well as finite temperature [4,5]. The first studies of spectral functions based on the MEM approach [6–13] have indeed been encouraging. These first studies, however, also showed that it is necessary to get control over typical lattice problems like finite cutoff effects or the influence of fermion doublers on the energy dependence (ω) of spectral functions. Cutoff effects show up in the large energy regime of spectral functions and one generally may not be too much worried about them when one is interested in extracting information about the low energy part of the spectral functions. This, however, is different for the analysis of properties of heavy quark bound states and they are also of particular importance for studies performed at finite temperature. In the latter case the high energy part of, e.g., the vector spectral function is directly related to physically observable dilepton cross sections and has been studied in much detail in (resumed) perturbative calculations [14]. Moreover, in the plasma phase of QCD quasiparticle excitations are heavy and typically will have masses that rise proportionally to the temperature. At high temperature this is expected to lead to broad resonancelike structures in spectral functions. In lattice calculations, which at present have all been performed with Wilson type fermion formulations, it is in general difficult to distinguish such effects from contributions arising from so-called heavy Wilson doublers. On a more technical level it is also important for the MEM analysis to include information on the short distance behavior of correlation functions in the default model. This requires information on lattice cutoff effects in the spectral function as well as possible modifications of the integration kernel.

There are apparently plenty of reasons to get control over the lattice cutoff effects in numerical calculations of spectral functions. We will analyze these in the infinite temperature limit of QCD by explicitly calculating hadronic spectral functions on lattices with finite temporal extent N_τ. We will present results for spectral functions calculated on isotropic as well as anisotropic lattices and discuss their quark mass dependence. Moreover, we will present results for standard Wilson fermions as well as for a truncated perfect action [15,16].

The paper is organized as follows. In Sec. II we summarize known results for free quark-antiquark spectral functions calculated in the continuum. In Sec. III we perform the corresponding calculation for Wilson fermions on the lattice. Section IV is devoted to a discussion of these lattice spectral functions, in particular, their quark mass and anisotropy dependence. In Sec. V we present results from a calculation with an improved Wilson fermion action, a truncated perfect action. Finally, we give our conclusions in Sec. VI. Some details of our calculations are presented in two Appendixes.

II. THERMAL QUARK-ANTIQUARK SPECTRAL FUNCTIONS

Thermal quark-antiquark correlation functions in coordinate space, $G_H(\tau,\vec{x})$, are defined as

$$G_H(\tau,\vec{x}) = \langle J_H(\tau,\vec{x}) J_H^\dagger(0,\vec{0})\rangle, \tag{2.1}$$

where $\langle\cdots\rangle$ denotes the thermal average. The local sources for currents with different mesonic quantum numbers H are given by $J_H(\tau,\vec{x}) = \overline{q}(\tau,\vec{x})\Gamma_H q(\tau,\vec{x})$, and Γ_H is an appropriate combination of γ matrices; i.e., $\Gamma_H = 1, \gamma_5, \gamma_\mu, \gamma_\mu\gamma_5$ for scalar, pseudoscalar, vector, and pseudovector channels, respectively. From these we obtain the mixed correlation functions at fixed momentum $\vec{p}$ which are commonly considered in lattice calculations,

$$G_H(\tau,\vec{p}) = \int d^3x G_H(\tau,\vec{x}) e^{i\vec{x}\vec{p}}. \tag{2.2}$$

These two-point functions have a spectral representation,

$$G_H(\tau,\vec{p}) = \int_0^\infty d\omega \sigma_H(\omega,\vec{p},T) K(\omega,\tau), \tag{2.3}$$

where $\sigma_H(\omega,\vec{p},T)$ denotes the temperature-dependent spectral function and $K(\omega,\tau)$ is the integration kernel which carries the entire dependence on Euclidean time $\tau \in [0,1/T)$,

$$K(\omega,\tau) = \frac{\cosh[\omega(\tau - 1/2T)]}{\sinh(\omega/2T)}. \tag{2.4}$$

It is easy to convince oneself that the spectral function appearing in Eq. (2.3) is indeed the Minkowski space spectral function (see, e.g., [17]):

$$\sigma_H(\omega,\vec{p},T) = \frac{1}{Z(T)} \sum_{n,m} e^{-E_n(\vec{p})/T}(1 - e^{-\omega/T}) \times \delta(\omega + E_n(\vec{p}) - E_m(\vec{p}))|\langle n|J_H(0)|m\rangle|^2, \tag{2.5}$$

where $Z(T)$ is the partition function and $\langle\cdots\rangle$ denotes here the matrix element of the hadronic current $J_H(0)$ taken between energy eigenstates at fixed momentum $\vec{p}$.

The correlation functions can be evaluated using the momentum space representation of the quark propagator and its spectral representation [17]. In the following, we will mainly be concerned with the zero momentum spectral functions $\sigma_H(\omega,T) \equiv \sigma_H(\omega,\vec{p}=\vec{0},T)$, which take on a rather simple form [17,18],

$$\sigma_H(\omega,T) = \frac{N_c}{8\pi^2}\Theta(\omega^2 - 4m^2)\omega^2 \tanh\left(\frac{\omega}{4T}\right) \times \sqrt{1 - \left(\frac{2m}{\omega}\right)^2}\left[a_H + \left(\frac{2m}{\omega}\right)^2 b_H\right] + \frac{N_c}{3}\frac{T^2}{2} f_H \omega \delta(\omega). \tag{2.6}$$

Here N_c denotes the number of colors, e.g., $N_c = 3$. For some selected mesonic quantum number channels H, the coefficients a_H, b_H, and f_H are given in Table I. We note that in some cases a contribution proportional to a δ function at vanishing energy appears in Eq. (2.6). At nonzero temperature this gives rise to a constant, τ-independent term in the Euclidean correlation function defined in Eq. (2.3). For massless quarks, also at nonvanishing momentum $p = \sqrt{\vec{p}^2}$, a rather compact form for the spectral function is obtained,

$$\sigma_H(\omega,\vec{p},T) = \frac{N_c}{8\pi^2}(\omega^2 - p^2)a_H\left\{\Theta(\omega^2 - p^2)\frac{2T}{p} \times \ln\frac{\cosh[(\omega+p)/4T]}{\cosh[(\omega-p)/4T]} + \Theta(p^2-\omega^2) \times \left[\frac{2T}{p}\ln\frac{\cosh[(p+\omega)/4T]}{\cosh[(p-\omega)/4T]} - \frac{\omega}{p}\right]\right\}. \tag{2.7}$$

Due to the asymptotic freedom of QCD the free field limit is approached at infinite temperature. In order to discuss the infinite temperature or free field limit of spectral functions and correlation functions it is appropriate to rescale all variables with nontrivial dimension by appropriate powers of the temperature, e.g., $\tilde{\omega} = \omega/T$. For fixed $\tilde{m} \equiv m/T$ the rescaled correlation functions $\tilde{G}_H(\tilde{\tau},\tilde{\vec{p}}) \equiv G_H(\tau T, \vec{p}/T)/T^3$ then have a well defined infinite temperature limit,

$$\tilde{G}_H(\tilde{\tau},\tilde{p}) = \int_0^\infty d\tilde{\omega}\tilde{\sigma}_H(\tilde{\omega},\tilde{\vec{p}},T)\tilde{K}(\tilde{\omega},\tilde{\tau}), \tag{2.8}$$

where $\tilde{\sigma}$ denotes the rescaled spectral density, $\tilde{\sigma}_H(\tilde{\omega},\tilde{\vec{p}},T) = \sigma_H(\omega,\vec{p},T)/T^2$, and

$$\tilde{K}(\tilde{\omega},\tilde{\tau}) = \cosh[\tilde{\omega}(\tilde{\tau} - 1/2)]/\sinh(\tilde{\omega}/2).$$

Eventually, we are interested in obtaining information on the temperature dependence of the physical spectrum and we thus want to determine the Minkowski space spectral function as introduced in Eq. (2.5). In the continuum the spectral function is connected to the temporal Euclidean correlation function via Eq. (2.3). The analyticity properties required to make that connection, however, in general exist only in the continuum. Therefore, extracting a spectral function from lattice data on Euclidean correlation functions via Eq. (2.3)

TABLE I. Coefficients a_H, b_H, and f_H for free spectral functions in different mesonic quantum number channels H [Eq. (2.6)]. The last two columns give coefficients appearing in the definition of the corresponding correlation functions on the lattice [Eq. (3.5)]. The momentum-dependent function d is defined in Eq. (3.7).

H	a_H	b_H	f_H	$c_H^{\rm lat}$	$d_H^{\rm lat}$
PS	1	0	0	1	0
S	-1	1	0	$-d$	$d-1$
V_0	0	0	-1	0	-1
$\Sigma_{i=1}^3 V_i$	2	1	1	$3-d$	d
$V \equiv \Sigma_{\mu=0}^3 V_\mu$	2	1	0	$3-d$	$d-1$
A_0	0	0	1	$1-d$	d
$\Sigma_{i=1}^3 A_i$	-2	3	-1	$-2d$	$2d-3$
$A \equiv \Sigma_{\mu=0}^3 A_\mu$	-2	3	0	$1-3d$	$3(d-1)$

will suffer from lattice artifacts and it is only in the continuum limit that a direct relation to the spectral properties at finite temperature can be established. This will become clear in the following section, where we discuss the spectral representation of mesonic correlation functions using the standard Wilson fermion formulation on Euclidean lattices with finite temporal extent N_τ.

III. LATTICE SPECTRAL FUNCTIONS WITH WILSON FERMIONS

In the following, the dimensionless representation of hadronic two-point correlation functions and the corresponding rescaled spectral functions given in Eq. (2.8) will be analyzed for their cutoff dependence. The situation here is similar to the discussion of the cutoff dependence of bulk thermodynamic variables, e.g., the rescaled pressure P/T^4 [1,19]. In that case, on isotropic lattices, deviations from the continuum result can be expressed in terms of the lattice spacing given in units of the temperature aT, which is nothing else but the inverse of the temporal extent of the lattice, $aT=1/N_\tau$. For bulk thermodynamic observables the temperature is in general the only[1] quantity with nontrivial dimension that can set the scale for the cutoff dependence. In the case of spectral functions, however, the energy provides another scale, and we can expect to find an additional dependence of the spectral functions on $a\omega=\tilde{\omega}/N_\tau$. However, we will show explicitly in the following that only $\tilde{\omega}/N_\tau$ determines the cutoff dependence and a sole dependence on $1/N_\tau$ does not appear in the spectral functions. On anisotropic lattices cutoff effects are, in addition, controlled by the ratio $\xi=a/a_\tau$ of spatial (a) and temporal (a_τ) lattice spacings. In this case, temperature and energy in (spatial) lattice units also depend on this ratio as $aT=\xi/N_\tau$ and $a\omega=\tilde{\omega}\xi/N_\tau$, respectively.

We will discuss here the cutoff dependence of spectral functions calculated within a generalization of Wilson's fermion discretization scheme [20] on anisotropic lattices. In the free field limit the fermion action is diagonal in the color degrees of freedom $S_F=\Sigma_{k,l}\Sigma_{c=1}^{3}\overline{\psi}_k^c Q_{k,l}\psi_l^c$ with the fermion matrix

$$Q_{k,l}=\left[r_\tau+\frac{3r+\hat{m}}{\xi}\right]\delta_{k,l}-\frac{1}{2}[(r_\tau-\gamma_0)\delta_{k+\hat{0},l}+(r_\tau+\gamma_0)\delta_{k-\hat{0},l}]-\frac{1}{2\xi}\sum_{i=1}^{3}[(r-\gamma_i)\delta_{k+\hat{i},l}+(r+\gamma_i)\delta_{k-\hat{i},l}], \tag{3.1}$$

where the dimensionless quark mass $\hat{m}$ is expressed in units of the spatial lattice spacing, $\hat{m}=ma$. The generic choice of the Wilson action is $r=r_\tau=1$ [20]. We will discuss here only the case $r_\tau=1$ as this avoids the occurrence of a second pole in the fermion propagator which would give rise to an unphysical timelike doubler mass. We will, however, consider the spacelike Wilson r parameter $r\in(0,1]$ as an additional free parameter of the fermion action. Even on anisotropic lattices with $\xi>1$ the generic choice for the r parameter is $r=1$. Yet, by choosing $r=1/\xi$, discretization errors of order ma can be completely eliminated at leading order from meson correlators with improved Wilson (clover) fermions on anisotropic lattices [21], e.g., in studies of heavy quark systems. As this choice has, in fact, been used in recent studies of heavy quark spectral functions [13], we also will explore the dependence of spectral functions on the choice of r.

Analytic results for the free field limit of hadronic correlation functions on isotropic lattices of size $N_\sigma^3\times N_\tau$ have been presented in the past using free Wilson fermions [22] with $r=1$. It is straightforward to extend these calculations to the case of anisotropic lattices and $r\neq 1$. The starting point for the calculation of hadronic correlation functions is the momentum space representation of the free Wilson fermion propagator,

$$S(k)=\frac{-i\gamma_0\sin k_0-i\mathcal{K}+[(1-\cos k_0)+\mathcal{M}]}{\sin^2 k_0+\mathcal{K}^2+[(1-\cos k_0)+\mathcal{M}]^2} \tag{3.2}$$

with

$$\mathcal{K}=\frac{1}{\xi}\sum_{i=1}^{3}\gamma_i\sin k_i, \tag{3.3}$$

$$\mathcal{M}=\frac{1}{\xi}\left[r\sum_{i=1}^{3}(1-\cos k_i)+\hat{m}\right]. \tag{3.4}$$

On a finite lattice of size $N_\sigma^3\times N_\tau$ the momenta take on discrete values, $k_0=(2\pi/N_\tau)(n_0+1/2)$ with $n_0=0,\ \pm 1,\ldots,\pm(N_\tau/2-1),\ N_\tau/2$ and $k_i=(2\pi/N_\sigma)n_i$ with $n_i=0,\ \pm 1,\ldots,\pm(N_\sigma/2-1),\ N_\sigma/2$ for $i=1,2,3$.

Following Ref. [22] one finds for the temporal zero momentum free quark-antiquark correlation functions with mesonic quantum numbers H,

$$\tilde{G}_H(\tilde{\tau},\tilde{p}\equiv 0)=N_c\left(\frac{N_\tau}{\xi N_\sigma}\right)^3\sum_{\vec{k}}\frac{c_H^{\mathrm{lat}}(\vec{k})\cosh[2E(\vec{k})N_\tau(\tilde{\tau}-1/2)]+d_H^{\mathrm{lat}}(\vec{k})}{(1+\mathcal{M})^2\cosh^2[E(\vec{k})N_\tau/2]}, \tag{3.5}$$

[1]This is correct in the limit of vanishing as well as infinite quark masses.

which is defined on the discrete set of Euclidean times $\tilde{\tau} = n/N_\tau$, with $n=0, 1, \ldots, N_\tau - 1$, accessible on a lattice with temporal extent N_τ. The energy $E \equiv E(\vec{k})$ is given by the location of the pole of the denominator of the Wilson fermion propagator [Eq. (3.2)] at $ik_0 = E(\vec{k})$, i.e.,

$$\cosh E = 1 + \frac{\mathcal{K}^2 + \mathcal{M}^2}{2(1+\mathcal{M})}. \tag{3.6}$$

The functions $c_H^{\rm lat}$ and $d_H^{\rm lat}$ appearing in Eq. (3.5) depend on the three-momentum $\vec{k}$ through the function

$$d \equiv d(\vec{k}) = \frac{\mathcal{K}^2}{\sinh^2 E}. \tag{3.7}$$

Note that d approaches 1 in the continuum limit. For some quantum number channels explicit expressions are given in Table I.

Equations (3.5)–(3.7) can be used to analyze the infinite temperature limit of mesonic correlation functions on any finite lattice of size $N_\sigma^3 \times N_\tau$. In the following, we will take the thermodynamic limit[2] ($N_\sigma \to \infty$) and concentrate on the cutoff dependence of these correlation functions which arises from N_τ being finite. In the thermodynamic limit the momenta are continuously distributed in the interval $[-\pi, \pi]$ and the energy consequently becomes a continuous function. This allows for an integral representation of Euclidean correlation functions in complete analogy to the continuum representation given in Eq. (2.3). In particular, we will show that on lattices with finite temporal extent N_τ also the integration kernel is identical to the continuum kernel, Eq. (2.4). Cutoff effects that are responsible for the deviation of the lattice correlation functions from the corresponding continuum correlation functions thus show up only in the lattice spectral functions.

In the thermodynamic limit, the momentum sum appearing in Eq. (3.5) gets replaced by a three-dimensional integral over the lattice Brillouin zone,

$$\frac{1}{N_\sigma^3} \sum_{\vec{k}} \to \int_{\vec{k}} \equiv \frac{1}{(2\pi)^3} \int \int \int_{-\pi}^{\pi} d^3k.$$

It is obvious from Eq. (3.5) and Table I that there will appear only two types of τ-dependent integrals which result from the two terms appearing in the definition of $c_H^{\rm lat}$, i.e., 1 and $d(\vec{k})$, respectively,

$$\tilde{G}_1(\tilde{\tau}) = N_c \left(\frac{N_\tau}{\xi}\right)^3 \int_{\vec{k}} \frac{1}{(1+\mathcal{M})^2} \frac{\cosh[2E(\vec{k})N_\tau(\tilde{\tau}-1/2)]}{\cosh^2[E(\vec{k})N_\tau/2]},$$

$$\tilde{G}_2(\tilde{\tau}) = N_c \left(\frac{N_\tau}{\xi}\right)^3 \int_{\vec{k}} \frac{d(\vec{k})}{(1+\mathcal{M})^2} \frac{\cosh[2E(\vec{k})N_\tau(\tilde{\tau}-1/2)]}{\cosh^2[E(\vec{k})N_\tau/2]}. \tag{3.8}$$

[2]In general we found that the dependence on the spatial extent becomes weak for $\xi N_\sigma / N_\tau \gtrsim 3$.

In addition there are also two τ-independent integrals related to the sums involving the term $d_H^{\rm lat}$ appearing in Eq. (3.5). These constants contribute to the δ functions at vanishing frequency. On finite lattices all quantum number channels listed in Table I (except the pseudoscalar) will receive non-vanishing contributions $f_H^{\rm lat}$,

$$f_H^{\rm lat} = N_c \left(\frac{N_\tau}{\xi}\right)^3 \int_{\vec{k}} \frac{d_H^{\rm lat}(\vec{k})}{(1+\mathcal{M})^2} \frac{1}{\cosh^2[E(\vec{k})N_\tau/2]}. \tag{3.9}$$

The integrals given in Eq. (3.8) are the starting point for our discussion of the cutoff dependence of mesonic spectral functions. So far we have achieved a representation of the correlation functions $\tilde{G}_H(\tilde{\tau})$ in terms of three-dimensional momentum integrals. Our goal is to find, for finite N_τ, a spectral representation defined through the one-dimensional integral given in Eq. (2.3). This can be achieved by introducing the energy in units of the temperature, $\tilde{\omega} = 2EN_\tau$, as one of the integration variables. In Appendix A we show explicitly for the case $r=1$ the sequence of variable transformations required to obtain an integral representation which is in complete analogy to the continuum relation Eq. (2.8), i.e., we can write the integrand of this integral as a product of a τ-independent *lattice spectral function* expressed in units of T^2 and a τ-dependent kernel which is identical with the continuum kernel $\tilde{K}$ defined in Eq. (2.4),

$$\tilde{G}_i(\tilde{\tau}) = \int_{\tilde{\omega}_{\rm min}}^{\tilde{\omega}_{\rm max}} d\tilde{\omega}\, \tilde{\sigma}_i(\tilde{\omega}, N_\tau) \tilde{K}(\tilde{\omega}, \tilde{\tau}), \quad i = 1,2. \tag{3.10}$$

The spectral functions $\tilde{\sigma}_i(\tilde{\omega}, N_\tau)$ explicitly depend on the lattice cutoff, which is reflected in the explicit dependence on $\tilde{\omega}/N_\tau = \omega a_\tau$,

$$\tilde{\sigma}_1(\tilde{\omega}, N_\tau) = \frac{N_c}{2\pi^3} \frac{N_\tau^2}{\xi^3} \tanh\left(\frac{\tilde{\omega}}{4}\right) \sinh\left(\frac{\tilde{\omega}}{4N_\tau}\right) \times \sinh\left(\frac{\tilde{\omega}}{2N_\tau}\right) I_1(\tilde{\omega}/N_\tau, \xi),$$

$$\tilde{\sigma}_2(\tilde{\omega}, N_\tau) = \frac{N_c}{2\pi^3} \frac{N_\tau^2}{\xi^3} \tanh\left(\frac{\tilde{\omega}}{4}\right) \frac{\sinh^3(\tilde{\omega}/4N_\tau)}{\sinh(\tilde{\omega}/2N_\tau)} \times I_2(\tilde{\omega}/N_\tau, \xi). \tag{3.11}$$

The two-dimensional integrals $I_i(\tilde{\omega}/N_\tau, \xi)$ are worked out in Appendix A for the case $r=1$. They can, however, also be defined for arbitrary values of r.

The integration limits in Eq. (3.10) depend on the quark mass, the anisotropy, and the Wilson r parameter. For $r=1$ the maximal energy is determined by the largest quark three-momentum possible, $\vec{k} = (\pi, \pi, \pi)$, and we find from Eq. (3.6)

$$\tilde{\omega}_{\rm min} = 2N_\tau \ln(1 + \hat{m}/\xi), \quad \tilde{\omega}_{\rm max} = 2N_\tau \ln[1 + (6 + \hat{m})/\xi]. \tag{3.12}$$

For $r<1$, however, the maximal energy generally corresponds to a momentum in the interior of the first Brillouin

zone. The corners of the three-dimensional Brillouin zone are local minima of the dispersion relation, which are interpreted as doubler masses proportional to the Wilson r parameter, i.e., they become lighter with decreasing r. As we will see, this leads to rather complicated spectral properties even in the free quark, infinite temperature limit.

We also note that the lattice spectral functions $\tilde{\sigma}_i$ are directly proportional to the massless spectral functions in the continuum $[\tilde{\sigma}_H \sim \tilde{\omega}^2 \tanh(\tilde{\omega}/4)]$. In the massless limit the deviations from the continuum results thus arise only through the ratio $\tilde{\omega}/N_\tau \equiv \omega a_\tau$, which is the energy expressed in units of the temporal lattice spacing. Equation (3.11) explicitly reflects a well known feature of the lattice formulation, i.e., cutoff effects depend on the energy scale. Of course, an explicit dependence on the lattice spacings (a, a_τ) never appears in the lattice formulation. It is, however, remarkable that no explicit dependence on $1/N_\tau \equiv a_\tau T$ appears in the spectral functions either.

Finally, we want to reconstruct from $\tilde{\sigma}_i$ the spectral functions in fixed quantum number channels. In particular, we will consider spectral functions in the pseudoscalar, scalar, vector, and axial-vector channels, which are given by

$$\tilde{\sigma}_{PS}^{\rm lat} = \tilde{\sigma}_1, \quad \tilde{\sigma}_S^{\rm lat} = -\tilde{\sigma}_2, \quad \tilde{\sigma}_V^{\rm lat} = 3\tilde{\sigma}_1 - \tilde{\sigma}_2,$$

$$\tilde{\sigma}_A^{\rm lat} = \tilde{\sigma}_1 - 3\tilde{\sigma}_2. \tag{3.13}$$

We ignore here a term proportional to $\tilde{\omega}\delta(\tilde{\omega})$ which, as discussed above, arises from the τ-independent part $(f_H^{\rm lat})$ of the correlation functions. For the above quantum number channels the coefficients of the δ functions will vanish in the continuum limit and we have checked that they are indeed already small on lattices with temporal extent $N_\tau \sim 10$.

IV. CUTOFF EFFECTS ON ISOTROPIC AND ANISOTROPIC LATTICES

We will analyze here in detail the lattice spectral functions derived in the previous section for some choices of parameters (r, ξ, m) which have been used in recent studies of meson spectral functions at finite temperature.

A. Massless quarks on isotropic lattices: $\xi = 1$, $m = 0$

Let us first discuss the lattice size dependence of the spectral functions for the case of vanishing quark masses ($m = 0$) and on isotropic lattices ($\xi = 1$). In Fig. 1(left) we show the ratios of the lattice and the corresponding continuum spectral functions. We note that this ratio is a function of $\tilde{\omega}/N_\tau \equiv \omega a$ only. The spectral functions vanish for $\tilde{\omega} \geq \tilde{\omega}_{\rm max}$, where $\tilde{\omega}_{\rm max}/N_\tau \equiv \omega_{\rm max} a = 2 \ln 7$ is obtained from Eq. (3.6) as the largest energy possible for a mesonic state constructed from two independent massless Wilson fermions with momentum $\vec{k} = (\pi, \pi, \pi)$. In the pseudoscalar and vector channels we observe a pronounced peak which occurs when the momenta of both Wilson fermions correspond to the first corner of the Brillouin zone $\vec{k} = (\pi, 0, 0)$. The corresponding energy is $\omega_1 a = 2 \ln 3$. Finally, we observe a cusp

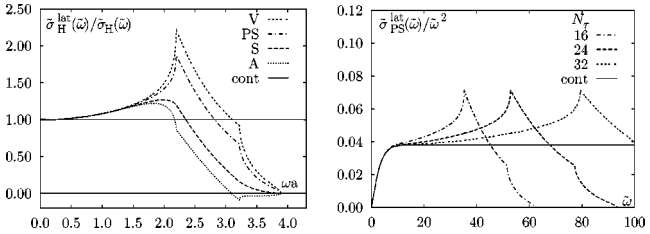

FIG. 1. Ratio of lattice and continuum spectral functions with $m = 0$ and $\xi = 1$ and for different quantum number channels (left). The figure on the right hand side shows the pseudoscalar lattice spectral functions calculated for lattices with temporal extent $N_\tau = 16$, 24, and 32. The solid line corresponds to the continuum spectral function given in Eq. (2.6).

at $\omega_2 a = 2 \ln 5$ between $\omega_1 a$ and $\omega_{\rm max} a$, which corresponds to the second corner of the Brillouin zone $\vec{k} = (\pi, \pi, 0)$. In the continuum limit the lattice artifacts shift to higher energies and the lattice spectral functions approach the continuum result [Fig. 1 (right)].[3]

In the interacting case also [6], a peaklike structure has been observed at similar values of the energy, i.e., for $\omega a \simeq 1.7$ in the pseudoscalar and $\omega a \simeq 2$ in the vector spectral function. It has been shown that these peaks shift to larger energies when the lattice spacing is decreased. They have thus been identified as lattice artifacts, which do not correspond to physical states in the continuum limit [6]. It is likely that these peaks are remnants of the cutoff effects seen here in the free spectral functions. To establish this relation in more detail it would certainly be interesting to analyze spectral functions in the scalar and axial-vector channels also. At least in the free case, the peaks that show up in the pseudoscalar and vector spectral functions are absent in the scalar and axial-vector channels.

In Ref. [6] it was suggested that the cutoff-dependent peaks in the spectral functions are related to bound states involving heavy quark doublers with masses of $\mathcal{O}(1/a)$. In view of the free spectral function we would, however, prefer not to speak of states at all. Rather, the distortion of the spectral function and the characteristic structures seen in the free case are due to the lattice dispersion relation and to the sudden restriction of available momentum space that occurs when one of the fermion momenta reaches one of the corners of the first Brillouin zone.

We also note that all four spectral functions coincide up to $\omega a \simeq 1.5$, where they differ by less than 15% from the continuum result. This agreement of different quantum number channels is reminiscent of the chiral symmetry of the free fermion action. In the lattice formulation with Wilson fermions, chiral symmetry is, of course, explicitly broken, which leads to different spectral functions in the scalar and pseudoscalar sectors. As can be seen from Fig. 1, this explicit breaking most strongly influences the large energy part of the spectrum, i.e., σ_{PS} deviates strongly from $-\sigma_S$ for $\omega a \gtrsim 1.5$. The same holds true in the vector and axial-vector

[3]Note that in the scalar and axial cases we always plot the positive functions $-\sigma_S$ and $-\sigma_A$.

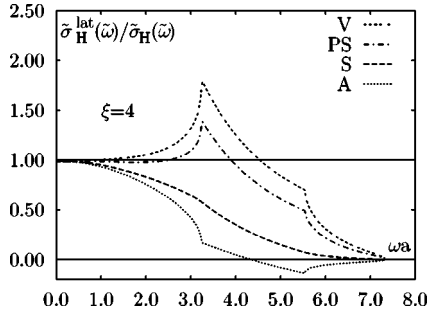

FIG. 2. Ratio of lattice and continuum spectral functions for $m=0$ and $\xi=4$.

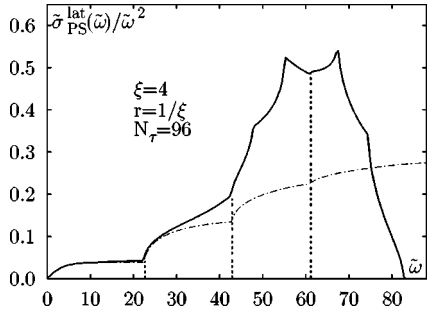

FIG. 3. Pseudoscalar lattice spectral function for massless quarks calculated on a lattice with temporal extent $N_\tau=96$ on an anisotropic lattice with $\xi=4$ and Wilson r parameter $r=1/\xi$ (solid curve). The dot-dashed curve shows the sum of contributions from continuum spectral functions for one massless pseudoscalar and a number of massive pseudoscalars constructed from free quarks with masses corresponding to the doubler masses obtained from the quark dispersion relation of this action. The horizontal lines indicate the locations of doubler masses in three distinct corners of the first Brillouin zone.

channels. Also note that for large energies the finite cutoff effects can lead to a negative lattice spectral function in the axial-vector channel.

B. Massless quarks on anisotropic lattices: $\xi>1$, $m=0$

When reducing the temporal relative to the spatial lattice spacing ($\xi=a/a_\tau>1$), one has to increase the number of grid points in the temporal direction if one wants to keep the temperature constant, $1/T=N_\tau a_\tau$. In the interacting case it requires a fine-tuning of spatial and temporal couplings (hopping parameter) to maintain rotational symmetry at zero temperature and, of course, it will also increase the computational effort. Nonetheless, it may be of advantage in the analysis of mesonic correlation functions at high temperature because one can make use of information on the correlation functions at a larger number of Euclidean time steps.

$r=1$

Let us first discuss the structure of free spectral functions on anisotropic lattices for the case $r=1$. As can be seen from Eq. (3.12), for a fixed ratio $\xi/N_\tau\equiv Ta$ the support for the spectral function increases with increasing anisotropy. For $(N_\tau,\xi)\to\infty$ it reaches a finite limit, i.e., $\tilde{\omega}_{\rm min}\to 2\tilde{m}$ and $\tilde{\omega}_{\rm max}\to 12N_\tau/\xi+2\tilde{m}$. By increasing the temporal lattice size and the anisotropy simultaneously, the upper limit, above which the spectral functions vanish, can thus be increased by about a factor of 3 relative to the case of isotropic lattices. For a moderate anisotropy factor ($\xi\simeq 4$), typically used in numerical calculations, $\tilde{\omega}_{\rm max}$ (and thus also $\omega_{\rm max}a$) is about a factor of 2 larger than in the isotropic case. Lattice artifacts, however, set in earlier; for $\xi=4$ the peak in the pseudoscalar and vector spectral functions is shifted only by a factor of 1.4 (see Fig. 2).

In Fig. 2 we show the same spectral functions as in Fig. 1 but now calculated with an anisotropy $\xi=4$, a choice of the anisotropy parameter which has been used in recent studies of spectral functions [12,13]. As can be seen from this figure the energy interval in which the pseudoscalar and vector spectral functions are only slightly affected by cutoff effects is about twice as large as on the isotropic lattices. The scalar and pseudoscalar correlation functions, however, are affected differently. As a consequence the degeneracy of both spectral functions, a precursor of chiral symmetry restoration, is lifted at smaller energies than on isotropic lattices. The situation is similar for the vector and axial-vector spectral functions.

$r=1/\xi$

When one uses the particular choice $r=1/\xi$ [13], the doubler masses become light for large ξ and can influence the spectral properties at lower energies than is the case for $r=1$. As the quark dispersion relation no longer leads to maxima in the corners of the Brillouin zone, the energy range in which the spectral functions are nonzero shrinks compared to the $r=1$ case. For $\xi=1/r=4$ one finds from the quark dispersion relation $\omega_{\rm max}a=3.45$, which is even slightly smaller than the corresponding value for $r=\xi=1$.

The nonmonotonic behavior of the dispersion relation also makes it more complicated to find a closed analytic representation for the spectral functions in terms of two-dimensional integrals, as we did for the case $r=1$. Although in principle it is possible to generalize the approach described in Appendix A for $r=1$, in the case $r<1$ we have used the simpler numerical binning approach to calculate spectral functions. This is also introduced in Appendix A. The resulting pseudoscalar spectral function is shown in Fig. 3 for massless quarks and $\xi=1/r=4$. In this case the mass of the lightest, threefold degenerate doubler is $m_1a=0.471$, which gives rise to the first threshold at $\tilde{\omega}_1=2N_\tau m_1 a/\xi$ seen in this figure. The other structures seen in this figure result from contributions of the doublers in the other corners of the Brillouin zone as well as the maxima of the quark dispersion relation, which now do not reside in the corners of the Brillouin zone.

We note that this action does reproduce the continuum spectral function well up to the point where the first doubler starts contributing, $\omega a\simeq 1$. The energy range in which a good agreement with the continuum spectral function can be achieved is thus compatible with the isotropic case.

C. Massive quarks

The modification of heavy quark bound states and, in particular, their dissolution in a quark-gluon plasma is consid-

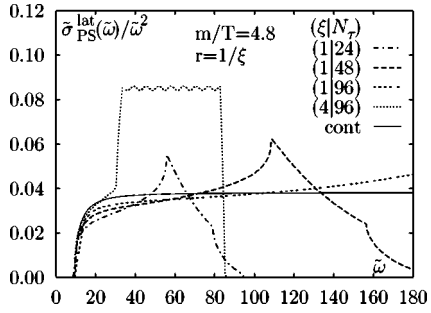

FIG. 4. Free pseudoscalar spectral functions for fixed m/T calculated on isotropic lattices with different temporal extents and quark masses. Also shown is the result obtained on an anisotropic lattice with $\xi=1/r=4$. In this case the spectral function deviates strongly from the continuum result for $\tilde{\omega}\gtrsim 30$ (see also Fig. 3). For better visibility we have cut out this part here and replaced it by a wavy line.

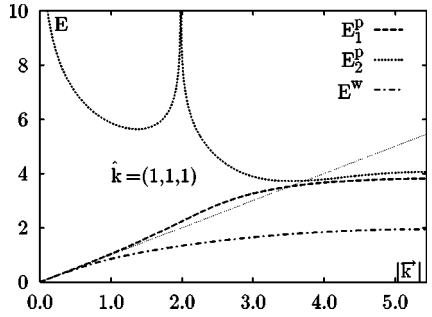

FIG. 5. The physical (E_1^p) and unphysical (E_2^p) poles of the quark propagator obtained from the truncated perfect action as functions of the spatial momentum $\vec{k}$. The straight line shows the continuum dispersion relation and the dash-dotted curve gives the dispersion relation for the standard Wilson fermion action (E^w).

ered to be an important signature for the formation of dense matter in heavy ion collisions. It thus is of interest to analyze spectral functions for heavy quark bound states also in lattice calculations. The first attempts to do so followed the strategies discussed in the previous sections, i.e., calculations have been performed with Wilson or clover fermions on isotropic [11] and anisotropic [13] lattices. In the latter case the formulation with $r=1/\xi$ was used.

The analysis presented in the previous sections for massless quarks also carries over to the case of massive quarks. The structure of the cutoff dependence discussed for the various types of actions follows patterns similar to those seen in the massless case. In the large energy region the cutoff effects dominate and a nonvanishing quark mass has little influence on the location of the pronounced peaks observed for $r=1$ or the additional thresholds arising for $r=1/\xi$. This is shown in Fig. 4, where we present results for quark masses $m/T=4.8$. Aside from the low energy threshold, which is now shifted to $\tilde{\omega}\simeq 2m/T$, the spectral functions are similar to those shown in Figs. 1 and 3.

V. LATTICE SPECTRAL FUNCTIONS WITH IMPROVED WILSON FERMIONS

In the previous sections we have seen that spectral functions obtained from calculations with the standard Wilson action reproduce the continuum spectral functions at low energies, $\omega a\lesssim 1.5$. Deviations from the continuum dispersion relation, however, lead to strong modifications of the spectral functions at larger energies. Moreover, the violation of chiral symmetry becomes visible in spectral functions at these energies. This motivates us to analyze the cutoff effects of hadron correlation functions computed with improved fermion actions, which have better chiral properties and lead to an improved dispersion relation. Much progress has been made in constructing such actions [23]. As a first step in this direction we want to analyze here a simple truncated version of a fixed point action [15,16]. This action is constructed from a small set of couplings which connect sites in an elementary hypercube of the lattice and can be handled in close analogy to the case of the Wilson action. We restrict ourselves to discussion of the massless case on isotropic lattices. The action can be written as

$$S=\sum_{x,y}\overline{\psi}(x)\left\{\sum_{\mu=0}^{3}\gamma_\mu\rho_\mu(x-y)+\lambda(x-y)\right\}\psi(y), \tag{5.1}$$

with

$$\begin{aligned}\rho_\mu(x-y)=&\rho_1(\delta_{y,x+\hat{\mu}}-\delta_{y,x-\hat{\mu}})+\sum_{\hat{\nu}\neq\hat{\mu}}\rho_2(\delta_{y,x+\hat{\mu}+\hat{\nu}}\\&-\delta_{y,x-\hat{\mu}+\hat{\nu}})+\sum_{\substack{\hat{\nu}\neq\hat{\mu}\\ \hat{\rho}\neq\hat{\mu},\hat{\nu}}}\rho_3(\delta_{y,x+\hat{\mu}+\hat{\nu}+\hat{\rho}}\\&-\delta_{y,x-\hat{\mu}+\hat{\nu}+\hat{\rho}})+\sum_{\substack{\hat{\nu}\neq\hat{\mu}\\ \hat{\rho}\neq\hat{\nu},\hat{\sigma}\neq\hat{\rho}}}\rho_4(\delta_{y,x+\hat{\mu}+\hat{\nu}+\hat{\rho}+\hat{\sigma}\\&-\delta_{y,x-\hat{\mu}+\hat{\nu}+\hat{\rho}+\hat{\sigma}}),\end{aligned} \tag{5.2}$$

$$\begin{aligned}\lambda(x-y)=&\lambda_0\delta_{y,x}+\sum_{\mu}\lambda_1(\delta_{y,x+\hat{\mu}}+\delta_{y,x-\hat{\mu}})\\&+\sum_{\hat{\nu}\neq\hat{\mu}}\lambda_2(\delta_{y,x+\hat{\mu}+\hat{\nu}}+\delta_{y,x-\hat{\mu}+\hat{\nu}})\\&+\sum_{\substack{\hat{\nu}\neq\hat{\mu}\\ \hat{\rho}\neq\hat{\mu},\hat{\nu}}}\lambda_3(\delta_{y,x+\hat{\mu}+\hat{\nu}+\hat{\rho}}+\delta_{y,x-\hat{\mu}+\hat{\nu}+\hat{\rho}})\\&+\sum_{\substack{\hat{\nu}\neq\hat{\mu}\\ \hat{\rho}\neq\hat{\nu},\hat{\sigma}\neq\hat{\rho}}}\lambda_4(\delta_{y,x+\hat{\mu}+\hat{\nu}+\hat{\rho}+\hat{\sigma}}+\delta_{y,x-\hat{\mu}+\hat{\nu}+\hat{\rho}+\hat{\sigma}}).\end{aligned} \tag{5.3}$$

Here, $\hat{\mu},\hat{\nu},\hat{\rho}$, and $\hat{\sigma}$ denote unit vectors along positive as well as (except for $\hat{\mu}$) negative directions in the hypercubic lattice. Numerical values for the set of nine couplings $\{\rho_i\}_{i=1}^4$, $\{\lambda_i\}_{i=0}^4$ are given in Table 1 of [16] for $m=0$.

Taking the Fourier transform of the action Eq. (5.1), it is straightforward to write down the propagator in momentum space:

$$S(k)=\frac{-i\gamma_0\delta\sin k_0-i\mathcal{K}_1-i\mathcal{K}_2\cos k_0+\kappa_1+\kappa_2\cos k_0}{(\mathcal{K}_1^2+\kappa_1^2+\delta^2)+2\cos k_0(\mathcal{K}_1\mathcal{K}_2+\kappa_1\kappa_2)+\cos^2 k_0(\mathcal{K}_2^2+\kappa_2^2-\delta^2)}, \tag{5.4}$$

with

$$\mathcal{K}_1=\sum_{i=1}^{3}\gamma_i\alpha_i, \quad \mathcal{K}_2=\sum_{i=1}^{3}\gamma_i\beta_i. \tag{5.5}$$

Explicit expressions for the momentum-dependent functions $\alpha_i=\alpha_i(\vec{k})$, $\beta_i=\beta_i(\vec{k})$, $\delta=\delta(\vec{k})$, $\kappa_1=\kappa_1(\vec{k})$, and $\kappa_2=\kappa_2(\vec{k})$ are given in Appendix B.

For the analysis of meson correlation functions and their spectral representation, one has to calculate the quark propagator in the mixed $(\tau,\vec{k})$ representation. The calculational steps are completely analogous to those for the standard Wilson action presented in Ref. [22]. However, the quark propagator now has two poles, $ik_0=E_i$. This is similar to the case of the Wilson action with $r_\tau<1$. The two poles are determined from

$$\cosh E_1=\frac{-P-\sqrt{(P^2-QR)}}{Q}, \tag{5.6}$$

$$\mathrm{sgn}(Q)\cosh E_2=\frac{-P+\sqrt{(P^2-QR)}}{Q}, \tag{5.7}$$

with additional functions

$$P(\vec{k})=\mathcal{K}_1\mathcal{K}_2+\kappa_1\kappa_2, \quad Q(\vec{k})=\mathcal{K}_2^2+\kappa_2^2-\delta^2,$$
$$R(\vec{k})=\mathcal{K}_1^2+\kappa_1^2+\delta^2. \tag{5.8}$$

In the limit $N_\tau\to\infty$ the quark propagator is then given by

$$\begin{aligned}S_\infty(\tau,\vec{k})=&\frac{1}{2\sqrt{P^2-QR}\sinh E_1}[(\kappa_1-i\mathcal{K}_1)+(\kappa_2-i\mathcal{K}_2)\\&\times\cosh E_1+\gamma_4\delta\,\mathrm{sgn}(\tau)\sinh E_1]e^{-E_1\tau}\\&-\frac{(-1)^{\tau\Theta(-Q)}}{2\sqrt{P^2-QR}\sinh E_2}[(\kappa_1-i\mathcal{K}_1)\,\mathrm{sgn}(Q)\\&+(\kappa_2-i\mathcal{K}_2)\cosh E_2+\gamma_4\delta\,\mathrm{sgn}(\tau)\sinh E_2]e^{-E_2\tau}.\end{aligned} \tag{5.9}$$

The first term describes the propagation of a physical state with energy (dispersion relation) $E_1(\vec{k})$, while the second corresponds to an unphysical state, the analogue of the time doubler in the case of the Wilson action with $r_\tau<1$. In Fig. 5 we show E_1 and E_2 as functions of $\vec{k}$.

As one can see from the figure, $E_1(\vec{k})$ is very close to the continuum result for small and moderate momenta and E_2 is much larger than E_1. Only for momenta $|\vec{k}|>2.5$ is the gap between E_2 and E_1 getting small. This has important consequences for the meson correlators which will be discussed below. Following exactly the same procedure as for the Wilson action, the meson correlators for finite N_τ can be written as

$$\tilde{G}_H(\tilde{\tau},p\equiv 0)=N_c\left(\frac{N_\tau}{N_\sigma}\right)^3\sum_{\vec{k}}\frac{c_H^{\mathrm{lat},p}(\vec{k})\cosh[2E_1(\vec{k})N_\tau(\tilde{\tau}-1/2)]+d_H^{\mathrm{lat},p}(\vec{k})}{(P^2-QR)\cosh^2[E_1(\vec{k})N_\tau/2]}+\Delta G_H^{E_2}(\tilde{\tau}). \tag{5.10}$$

The functions $c_H^{\mathrm{lat},p}(\vec{k})$ and $d_H^{\mathrm{lat},p}(\vec{k})$ are given in Table II in terms of $\delta(\vec{k})$ and a new function $d^p(\vec{k})$,

$$d^p\equiv d^p(\vec{k})=\frac{(\mathcal{K}_1+\mathcal{K}_2\cosh E_1)^2}{\sinh^2 E_1}. \tag{5.11}$$

The term $\Delta G_H^{E_2}(\tilde{\tau})$ in Eq. (5.10) contains a contribution from the second pole E_2, and an explicit expression for it is given in Appendix B. As the energies E_2 are large, it turns out that this part leads to negligible contributions to the correlation functions except for very short distances $(\tilde{\tau}=0,1/N_\tau)$. Using the binning approach discussed in Appendix A, we have calculated the spectral functions numerically in different quantum number channels. Results for $N_\tau=24$ are shown in Fig. 6. The good chiral properties and agreement with the continuum result over a wide range of energies ($\omega a\sim 5$) are self-evident. The contribution of the physical pole (E_1^p) has also been calculated analytically, which can be done in complete analogy to the case of the Wilson action. This contribution alone is, as expected, indistinguishable from the complete result up to $\omega a\sim 5$ (Fig. 6).

VI. CONCLUSIONS

We have presented an explicit calculation of mesonic spectral functions in the infinite temperature limit of lattice QCD. We analyzed the cutoff dependence of spectral functions in different quantum number channels for the Wilson fermion action on isotropic as well as anisotropic lattices. We

TABLE II. The coefficients $c_H^{\mathrm{lat},p}$ and $d_H^{\mathrm{lat},p}$ appearing in Eq. (5.10). The functions d^p and δ are defined in Eqs. (5.11) and (B7), respectively.

H	$c_H^{\mathrm{lat},p}$	$d_H^{\mathrm{lat},p}$
PS	δ^2	0
S	$-d^p$	$d^p-\delta^2$
V_0	0	$-\delta^2$
$\Sigma_{i=1}^3 V_i$	$3\delta^2-d^p$	d^p
$\Sigma_{\mu=0}^3 V_\mu$	$3\delta^2-d^p$	$d^p-\delta^2$
A_0	δ^2-d^p	d^p
$\Sigma_{i=1}^3 A_i$	$-2d^p$	$2d^p-3\delta^2$
$\Sigma_{\mu=0}^3 A_\mu$	δ^2-3d^p	$3(d^p-\delta^2)$

find that the cutoff effects are of similar magnitude in both cases. The introduction of a Wilson r parameter less than unity, in particular the choice $r=1/\xi$, does not seem to lead to a significant reduction of cutoff effects.

Furthermore, we analyzed the spectral representation of mesonic correlation functions using a truncated perfect action. As expected, this does lead to a drastic improvement of the spectral functions; cutoff effects are shifted to the high energy regime and chiral symmetry is preserved in the low energy part of the spectral functions up to energies $\omega a \simeq 5$.

ACKNOWLEDGMENT

The work was supported by the DFG under grant FOR 339/2-1 and by the U.S. Department of Energy under Contract DE-AC02-98CH10886.

APPENDIX A: FREE MESONIC LATTICE SPECTRAL FUNCTIONS

We derive here the explicit form of the representation of the free mesonic lattice spectral functions given in Eq. (3.11). In particular, we give closed analytic expressions for the integrals $I_i(y,\xi)$ appearing in these equations for the case $r=1$ and discuss a representation in terms of finite Riemann sums, which is more convenient for dealing with the case $r<1$ or spectral functions resulting from more complicated actions, like the truncated perfect action analyzed in Sec. V.

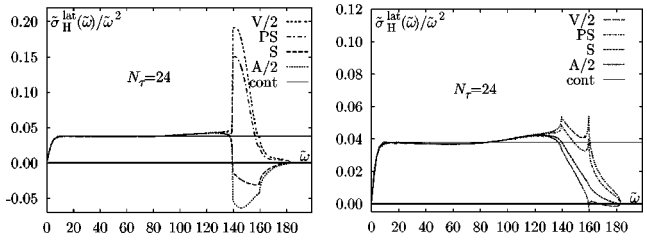

FIG. 6. Free spectral functions on isotropic lattices calculated with a truncated perfect action for $m=0$. The left figure shows the complete result, the right one the contribution from the physical pole (E_1^p) alone.

$r=1$

We start from Eq. (3.8) by performing the obvious variable transformation $\vec{k}\to\vec{x}=(\sin^2(k_1/2),\sin^2(k_2/2),\sin^2(k_3/2))$. We then define

$$\alpha=\frac{\mathcal{K}^2+\mathcal{M}^2}{4(1+\mathcal{M})} \tag{A1}$$

and rewrite Eq. (3.6) as $E=2\ln(\sqrt{\alpha}+\sqrt{1+\alpha})$. Using these expressions we can perform a second variable transformation, $\vec{x}\to(\tilde{\omega},z_2,z_3)=(2N_\tau E,x_2/\alpha,x_3/\alpha)$. This leads to the representation of the correlation functions $\tilde{G}_i$ [Eq. (3.10)] where the integrals $I_i(y,\xi)$ [Eq. (3.11)] are given by

$$I_i(y,\xi)=\int\int_{\Omega(y)} dz_2 dz_3 A(\vec{z})B(\vec{z})C_i(\vec{z}), \tag{A2}$$

with $\vec{z}=(z,z_2,z_3)$ and $z(y)=\sinh^2(y/4)$. We further define

$$x=\frac{\xi^2-(z_2+z_3)(1-2\xi z+\hat{m})+\xi\hat{m}-\hat{m}^2/4z-2zz_2z_3}{1+2z(z_2+z_3)+\hat{m}-2\xi z}. \tag{A3}$$

With this, the functions appearing in the integrand of I_i can be written as

$$A(\vec{z})=\xi\frac{\xi+2z(x+z_2+z_3)+\hat{m}}{1+2z(z_2+z_3)+\hat{m}-2\xi z}, \tag{A4}$$

$$B(\vec{z})=[1+2\xi^{-1}z(x+z_2+z_3)+\xi^{-1}\hat{m}]^{-2}, \tag{A5}$$

$$C_1(\vec{z})=[xz_2z_3(1-zx)(1-zz_2)(1-zz_3)]^{-1/2}, \tag{A6}$$

$$C_2(\vec{z})=\frac{4}{\xi^2}\frac{x(1-zx)+z_2(1-zz_2)+z_3(1-zz_3)}{[xz_2z_3(1-zx)(1-zz_2)(1-zz_3)]^{1/2}}. \tag{A7}$$

The boundary of the two-dimensional integration region, $\Omega(y)$, is given by

$$\Omega(y)=\{z_2,z_3|0\leqslant xy\leqslant 1;\ 0\leqslant z_2y\leqslant 1;\ 0\leqslant z_3y\leqslant 1\}. \tag{A8}$$

Arbitrary r

In general we can also determine the spectral function in a given quantum number channel directly from the representation of the correlation functions in Eq. (3.5). We can divide the interval of nonvanishing energies, $\tilde{\omega}=2N_\tau E(\vec{k})$, into n bins. Denoting by ω_i the central values of these bins and introducing the bin length $\epsilon=(\tilde{\omega}_{\max}-\tilde{\omega}_{\min})/n$, we can approximate Eq. (3.5) by

$$\tilde{G}_H(\tilde{\tau},\tilde{p}\equiv 0)\simeq\sum_{i=1}^{n}\epsilon s_i\frac{\cosh[\tilde{\omega}_i(\tilde{\tau}-1/2)]}{\sinh(\tilde{\omega}_i/2)}, \tag{A9}$$

TABLE III. The explicit form of the functions $g_H^{\mathrm{lat},p}$ appearing in Eq. (B13). The functions $d_1^{p3}(\vec{k})$ and $d_2^{p3}(\vec{k})$ are defined in Eqs. (B14) and (B15).

H	$g_H^{\mathrm{lat},p}$
PS	$d_1^{p3}+d_2^{p3}$
S	$-d_1^{p3}+d_2^{p3}$
V_0	$d_1^{p3}+d_2^{p3}$
$\Sigma_{i=1}^3 V_i$	$d_1^{p3}+3d_2^{p3}$
$\Sigma_{\mu=0}^3 V_\mu$	$2d_1^{p3}+4d_2^{p3}$
A_0	$d_1^{p3}-d_2^{p3}$
$\Sigma_{i=1}^3 A_i$	$d_1^{p3}-3d_2^{p3}$
$\Sigma_{\mu=0}^3 A_\mu$	$2d_1^{p3}-4d_2^{p3}$

where s_i receives contributions from all terms in the momentum sum that lead to energies $2N_\tau E(\vec{k})$ in the ith bin,

$$s_i = N_c\left(\frac{N_\tau}{\xi N_\sigma}\right)^3 \sum_{\vec{k}} \Theta(2N_\tau E(\vec{k}) - (n-1)\epsilon) \times \Theta(n\epsilon - 2N_\tau E(\vec{k})) \frac{c_H^{\mathrm{lat}}(\vec{k})\sinh[N_\tau E(\vec{k})]}{(1+\mathcal{M})^2\cosh^2[E(\vec{k})N_\tau/2]}. \tag{A10}$$

In the limit of large spatial volumes ($N_\sigma \to \infty$) and small bin sizes ($\epsilon \to 0$), this gives the spectral functions in a given quantum number channel. We have used this approach to calculate spectral functions in the case $r<1$ and also in the case of the truncated perfect action. Typically, we used $N_\sigma \sim 1000$ and $n=1000$.

APPENDIX B: TRUNCATED PERFECT ACTION

In this appendix we give explicit expressions for the auxiliary functions that appear in calculations with the truncated perfect action, in particular in the quark propagator given in Eq. (5.4).

The explicit forms of the functions $\alpha_i(\vec{k})$, $\beta_i(\vec{k})$, $i=1,2,3$, and $\delta(\vec{k})$, $\kappa_1(\vec{k})$, and $\kappa_2(\vec{k})$ are given below:

$$\alpha_1(\vec{k}) = 2\hat{s}_1(\rho_1 + 2\rho_2(\hat{c}_2+\hat{c}_3) + 4\rho_3\hat{c}_2\hat{c}_3), \tag{B1}$$

$$\alpha_2(\vec{k}) = 2\hat{s}_2(\rho_1 + 2\rho_2(\hat{c}_1+\hat{c}_3) + 4\rho_3\hat{c}_1\hat{c}_3), \tag{B2}$$

$$\alpha_3(\vec{k}) = 2\hat{s}_3(\rho_1 + 2\rho_2(\hat{c}_1+\hat{c}_2) + 4\rho_3\hat{c}_1\hat{c}_2), \tag{B3}$$

$$\beta_1(\vec{k}) = 4\hat{s}_1[\rho_2 + 2\rho_3(\hat{c}_2+\hat{c}_3) + 4\rho_4\hat{c}_2\hat{c}_3], \tag{B4}$$

$$\beta_2(\vec{k}) = 4\hat{s}_2[\rho_2 + 2\rho_3(\hat{c}_1+\hat{c}_3) + 4\rho_4\hat{c}_1\hat{c}_3], \tag{B5}$$

$$\beta_3(\vec{k}) = 4\hat{s}_3[\rho_2 + 2\rho_3(\hat{c}_1+\hat{c}_2) + 4\rho_4\hat{c}_1\hat{c}_2], \tag{B6}$$

$$\delta(\vec{k}) = 2\rho_1 + 4\rho_2(\hat{c}_1+\hat{c}_2+\hat{c}_3) + 8\rho_3(\hat{c}_1\hat{c}_2+\hat{c}_2\hat{c}_3+\hat{c}_1\hat{c}_3) + 16\rho_4\hat{c}_1\hat{c}_2\hat{c}_3, \tag{B7}$$

$$\kappa_1(\vec{k}) = \lambda_0 + 2\lambda_1(\hat{c}_1+\hat{c}_2+\hat{c}_3) + 4\lambda_2(\hat{c}_1\hat{c}_2+\hat{c}_2\hat{c}_3+\hat{c}_1\hat{c}_3) + 8\lambda_3\hat{c}_1\hat{c}_2\hat{c}_3, \tag{B8}$$

$$\kappa_2(\vec{k}) = 2\lambda_1 + 4\lambda_2(\hat{c}_1+\hat{c}_2+\hat{c}_3) + 8\lambda_3(\hat{c}_1\hat{c}_2+\hat{c}_2\hat{c}_3+\hat{c}_1\hat{c}_3) + 16\lambda_4\hat{c}_1\hat{c}_2\hat{c}_3, \tag{B9}$$

where we introduced the shorthand notation $\hat{c}_i = \cos k_i$ and $\hat{s}_i = \sin k_i$.

Furthermore, we give the explicit expression for the term in the meson correlator $\Delta G_H^{E_2}(\tilde{\tau})$ coming from contributions of the second pole E_2. It can be written as

$$\Delta G_H^{E_2}(\tilde{\tau}) = G_{H2}(\tilde{\tau}) + G_{H12}(\tilde{\tau}), \tag{B10}$$

where $G_{H2}(\tilde{\tau})$ contains contributions from the second pole $ik_0 = E_2$ only and therefore can be written down in close analogy with the term containing only the contribution from the first pole E_1:

$$\tilde{G}_{H2}(\tilde{\tau}, \tilde{p}\equiv 0) = N_c\left(\frac{N_\tau}{N_\sigma}\right)^3 \sum_{\vec{k}} \frac{c_H^{\mathrm{lat},p2}(\vec{k})\cosh[2E_2(\vec{k})N_\tau(\tilde{\tau}-1/2)] + d_H^{\mathrm{lat},p2}(\vec{k})}{(P^2-QR)\cosh^2[E_2(\vec{k})N_\tau/2]}. \tag{B11}$$

The functions P,Q,R have been defined in Eq. (5.8); $d_H^{\mathrm{lat},p2}$ and $c_H^{\mathrm{lat},p2}$ have exactly the same structures as $d_H^{\mathrm{lat},p}$ and $c_H^{\mathrm{lat},p}$ listed in Table II with d^p being replaced by

$$d^{p2} \equiv d^{p2}(\vec{k}) = \frac{[\mathcal{K}_1 + \mathcal{K}_2 \mathrm{sgn}(Q)\cosh E_2]^2}{\sinh^2 E_2}. \tag{B12}$$

The second term $G_{H12}(\tilde{\tau})$ contains contributions from both the first and second poles and can be written as

$$G_{H12}(\tilde{\tau}) = N_c \left(\frac{N_\tau}{N_\sigma}\right)^3 \sum_{\vec{k}} \frac{(-1)^{\Theta(-Q)\tau+1}}{(P^2-QR)\cosh[E_1(\vec{k})N_\tau/2]\cosh[E_2(\vec{k})N_\tau/2]} [g_H^{\mathrm{lat},p}(\vec{k})\{\cosh[E_s(\vec{k})N_\tau(\tilde{\tau}-1/2)] - \cosh[E_d(\vec{k})N_\tau(\tilde{\tau} - 1/2)]\} + \delta^2(\vec{k})\{\cosh[E_s(\vec{k})N_\tau(\tilde{\tau}-1/2)] + \cosh[E_d(\vec{k})N_\tau(\tilde{\tau}-1/2)]\}], \tag{B13}$$

where $E_s = E_1 + E_2$, $E_d = E_1 - E_2$. An additional function $g_H^{\mathrm{lat},p}(\vec{k})$ has been introduced, which depends on

$$d_1^{p3} = \frac{\mathcal{K}_1^2 \mathrm{sgn}(Q) + \mathcal{K}_2^2 \cosh E_1 \cosh E_2 + \mathcal{K}_1\mathcal{K}_2[\cosh E_2 + \mathrm{sgn}(Q)\cosh E_1]}{\sinh E_1 \sinh E_2}, \tag{B14}$$

$$d_2^{p3} = \frac{\kappa_1^2 \mathrm{sgn}(Q) + \kappa_2^2 \cosh E_1 \cosh E_2 + \kappa_1\kappa_2[\cosh E_2 + \mathrm{sgn}(Q)\cosh E_1]}{\sinh E_1 \sinh E_2}. \tag{B15}$$

The explicit form of $g_H^{\mathrm{lat},p}$ for different quantum numbers is given in Table III.

[1] J. Engels, F. Karsch, and H. Satz, Nucl. Phys. **B205**, 239 (1982).
[2] Y. Nakahara, M. Asakawa, and T. Hatsuda, Phys. Rev. D **60**, 091503 (1999).
[3] R.K. Bryan, Eur. Biophys. J. **18**, 165 (1990).
[4] M. Asakawa, T. Hatsuda, and Y. Nakahara, Prog. Part. Nucl. Phys. **46**, 459 (2001).
[5] F. Karsch and I. Wetzorke, in *Proceedings of the International Workshop on Strong and Electroweak Matter 2000*, edited by C.P. Korthals-Altes (World Scientific, Singapore, 2001), hep-lat/0008008.
[6] CP-PACS Collaboration, T. Yamazaki *et al.*, Phys. Rev. D **65**, 014501 (2002).
[7] I. Wetzorke *et al.*, Nucl. Phys. B (Proc. Suppl.) **106**, 510 (2002); P. Petreczky *et al.*, *ibid.* **106**, 513 (2002).
[8] F. Karsch, E. Laermann, P. Petreczky, S. Stickan, and I. Wetzorke, Phys. Lett. B **530**, 147 (2002).
[9] C.R Allton *et al.*, Phys. Rev. D **66**, 094511 (2002); J. Clowser and C.G. Strouthos, Nucl. Phys. B (Proc. Suppl.) **106**, 489 (2002).
[10] S. Sasaki, K. Sasaki, T. Hatsuda, and M. Asakawa, hep-lat/0209059.
[11] S. Datta, F. Karsch, P. Petreczky, and I. Wetzorke, hep-lat/0208012.
[12] M. Asakawa, T. Hatsuda, and Y. Nakahara, hep-lat/0208059.
[13] T. Umeda, K. Nomura, and H. Matsufuru, hep-lat/0211003.
[14] E. Braaten, R. Pisarski, and T. Yuan, Phys. Rev. Lett. **64**, 2242 (1990).
[15] W. Bietenholz and U.J. Wiese, Nucl. Phys. **B464**, 319 (1996).
[16] W. Bietenholz, R. Brower, S. Chandrasekharan, and U.J. Wiese, Nucl. Phys. B (Proc. Suppl.) **53**, 921 (1997).
[17] M. Le Bellac, *Thermal Field Theory* (Cambridge University Press, Cambridge, England, 1996).
[18] F. Karsch, M.H. Mustafa, and M.H. Thoma, Phys. Lett. B **497**, 249 (2001).
[19] B. Beinlich, F. Karsch, and E. Laermann, Nucl. Phys. **B462**, 415 (1996).
[20] K. Wilson, Phys. Rep. **23**, 331 (1976).
[21] J. Harada *et al.*, Phys. Rev. D **64**, 074501 (2001).
[22] D.B. Carpenter and C.F. Baillie, Nucl. Phys. **B260**, 103 (1985).
[23] C. Gattringer, hep-lat/0208056; C. Gattringer *et al.*, hep-lat/0209099, and references therein.